J Geod (2009) 83:161–174
DOI 10.1007/s00190-008-0249-2

ORIGINAL ARTICLE

A method of error adjustment for marine gravity with application to Mean Dynamic Topography in the northern North Atlantic

A. Hunegnaw · R. G. Hipkin · J. Edwards

Received: 19 February 2008 / Accepted: 14 July 2008 / Published online: 31 July 2008

Abstract International compilations of marine gravity, such as the International Gravity Bureau (BGI) contain tens of millions of point data. Lemoine et al. (The Development of the Joint NASA GSFC and the National Imagery and Mapping Agency (NIMA) Geopotential Model EGM96, NASA/TP-1998-206861) chose not to include any marine gravity in the construction of the global gravity model EGM96. Instead they used synthetic anomalies derived from altimetry, so that no independent information about Mean Dynamic Topography (MDT) can be deduced. Software has been developed not only to identify and correct those aspects of marine gravity data that are unreliable, but to do so in a way that can be applied to very large, ocean-wide data sets. First, we select only straight-line parts of ship-tracks and fit each one with a high-degree series of Chebyshev polynomials, whose misfit standard deviation is σ_{line} and measures the *random error* associated with point gravity data. Then, network adjustment determines how the gravity datum is offset for each survey. A free least squares adjustment minimises the gravity anomaly mismatch at line-crossing points, using σ_{line} to weight the estimate for each line. For a long, well crossed survey, the instrumental drift rate is also adjusted. For some 42,000 cross-over points in the northern Atlantic Ocean, network adjustment reduces the unweighted standard deviation of the cross-over errors from 4.03 to 1.58 mGal; when quality weighted, the statistic reduces from 1.32 to 0.39 mGal. The geodetic MDT is calculated combining the adjusted gravity anomalies and satellite altimetry, and a priori global ocean model through a new algorithm called the Iterative Combination Method. This paper reports a first demonstration that geodetic oceanography can characterise the details of basin wide ocean circulation with a resolution better than global ocean circulation models. The result matches regional models of ocean circulation from hydrography measurements (Geophys Res Lett 29:1896, 2002; J Geophys Res 108:3251, 2003).

Keywords Marine gravity · Network adjustment · Mean Dynamic Topography · Geostrophic currents

A. Hunegnaw (✉) · R. G. Hipkin · J. Edwards
School of GeoSciences, University of Edinburgh,
West Mains Road, Edinburgh EH9 3JW, UK
e-mail: Addisu.Hunegnaw@ed.ac.uk

1 Introduction

International compilations of marine gravity, such as those by the International Gravity Bureau (BGI) and the National Geophysical Data Centre (NGDC) include some tens of millions of point data. The compilers of the 1996 Earth Gravity Model (Lemoine et al. 1998) decided that marine gravity data were too unreliable to be included. One of the purposes of this paper is to mitigate these errors. Software has been developed not only to identify and correct those aspects of marine gravity data that are unreliable but to do so in a way that can be applied to very large, ocean-wide data sets with little manual intervention. These corrections are essential for computing a high precision geoid or Mean Dynamic Topography. Although synthetic free air gravity anomaly fields derived from sea surface satellite altimetry have become a widely used tool for investigating marine geophysics and tectonics, their derivation ignores some scales of sea surface topography, making them inconsistent with applications to oceanography and vertical reference systems. The CHAllenging Minisatellite Payload (CHAMP) (Reigber et al. 2003) and the twin Gravity Recovery and Climate, Experiment Mission (GRACE) (Tapley et al. 2004) have not reliably resolved scales shorter than ∼500 km. While the future

Gravity field and steady-state Ocean Circulation Explorer (GOCE) satellite (Drinkwater et al. 2003) will improve this resolution, marine and airborne surveys remain the only way of providing real gravity field information at short wavelengths. Marine gravity measurements are, in principle, very precise: military trials of a type of gravity sensor now commercially available achieved RMS cross-over errors of only 0.1–0.2 mGal in rough seas (Perrin 1995, personal communication). Bell and Watts (1986) have also shown cross-over errors of ±0.38 mGal using BGM-3 sea gravimeter. For a variety of reasons, the accuracy of marine gravity anomalies does not match this precision. Some relate to measuring gravity on an imperfectly stabilised platform, with others due to systematic instrument errors, cross-coupling, loosing reference to an absolute gravity datum and uncertainties in the navigation system. Errors in course directions and speed affect the Eötvös correction. Wessel and Watts (1988) and Torge (1989) review these problems. There are additionally gross errors and blunders in data collection and transcription, and geographic inadequacies in data coverage. In attempting to exploit existing data, there can also be the problem that not enough information has been included in the archive or that restrictions on access do not allow important components of the information to be recovered.

Our strategy involves pre-processing followed by cross-over network adjustment. Pre-processing aims to reduce the dynamical errors associated with course changes, smooth out high-frequency noise, and remove spikes and gross blunders. Cross-over network adjustment aims to remove the systematic effects of datum offsets, different gravity reference systems and drift in the gravity meter. We do not include 'track-shifting' (Nishimura and Forsyth 1988) parameters in the adjustment model to correct for navigational errors: with the information available from most archives, we do not see a rational way of doing so. The removal of different characteristics of error sources and minimisation of errors in marine gravimetric observations has been the subject of several studies both global and regional scales (Talwani 1971; Strang Van Hees 1983; Wessel and Watts 1988; Wessel 1989; Wenzel 1992; Matao 1995; Adjaout and Sarrailh 1997; Hwang et al. 2002; Denker and Ronald 2003; Catalao and Sevilla 2004).

This work was carried out as part of the Geoid and Ocean Circulation in the North Atlantic (GOCINA) project more recently extended to the Ocean Circulation and Transport Between North Atlantic and the Arctic Sea (OCTAS) project, which aimed to determine dynamic sea surface topography from the combination of GRACE data, surface and airborne gravity anomaly measurements, satellite altimetry and hydrographic information, in preparation for the launch of the gravity gradiometer satellite GOCE. The northern North Atlantic was used to test the new methodology because its coverage by surface ship gravity data is amongst the densest in the world (see Fig. 1). This part of the northern North Atlantic has

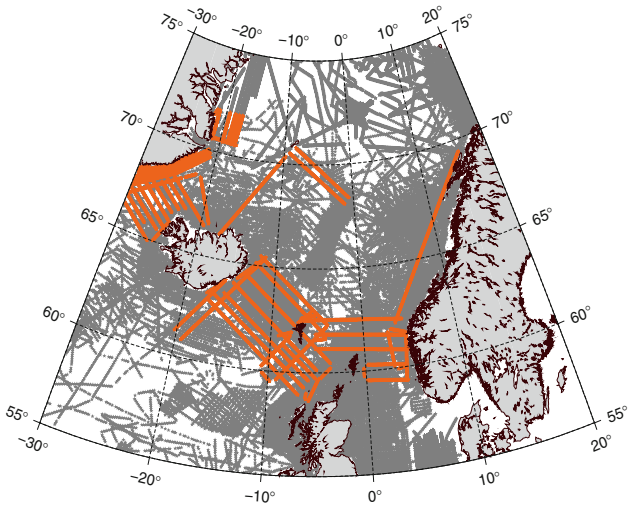

Fig. 1 Ship and airborne gravity data for the northern Atlantic, thinned to an along-track distance of 10 km. The airborne gravity profiles are shown in *red*. Land data not shown

benefited from a coincidence of oil exploration off the North West European shelf and the seminal role played by surveys of the Rejkjanes Ridge in the development of plate tectonics. Later academic interest in the Iceland hotspot, together with the Shetland–Faroes–Iceland–Greenland Ridge marking its bathymentric trail, extended detailed coverage beyond regions with petroleum potential. Finally some civilian benefit has derived from the intensive mapping of the northern Atlantic as a Cold-War submarine hide-away. Despite the unusually dense coverage of the gravity in the northern North Atlantic, a few regions remain far from the nearest observation. Computing a gravimetric geoid involves a surface integral of gravity, meaning that gravity coverage must be complete. Consequently, practical evaluation requires gravity to be interpolated into the gaps between survey lines. The cleaned and adjusted ship and airborne gravity data provides a strong constraint for surface gravity along survey lines. The interpolation process is then done by our algorithm called the Iterative Combination Method (ICM). It generates complete grids of gravity and MDT that are mutually consistent.

The geodetic MDT comes from modifying an initial a priori regional MDT model in two steps: first, we make its long wavelength structure consistent with satellite altimetry combined with the reliable parts of the geoid as deduced from GRACE observations; secondly, we add shorter wavelength information coming from the surface gravity data.

Our analysis has four stages: (1) data cleaning—identifying and cleaning every linear segment of ship tracks or aircraft flight lines (Sects. 3, 4, 5); (2) network adjustment—shifting the datum of every line segment to minimise the mismatch at points where tracks cross (to some long and well-connected surveys we include a drift parameter) (Sects. 6, 7, 8, 9, 10); (3) the ICM algorithm—filling gaps

between tracks and the resulting geodetic MDT (Sect. 11) and (4) validation—comparing the geostrophic flow field derived from the ICM MDT with independent data (Sect. 12). Finally, the summary and major conclusions are given in Sect. 13.

2 Gravity data in the northern North Atlantic

The main marine gravity data sets used in this study have been acquired from BGI, NGDC, Norwegian Mapping Agency (NMA), the Arctic Gravity Project (ArcGP) and from international and national oil companies, but we also had access on a restricted basis to the whole of British Geological Survey (BGS) data compilation covering British and Irish shelf waters. These data sets cover the area between latitudes of (45°N to 75°N) and longitudes of (75°W to 33°E).

The data were improved in 2003 by the GOCINA-OCTAS project, with a major airborne gravity survey campaign. The aircraft was equipped with GPS receivers, laser altimetry, Inertial Navigation Systems (INS), and a LaCoste and Romberg air–sea gravimeter. The long line connects between Greenland, Iceland, the Faroes, Shetland, the Hebrides, Norway and Jan Mayan. This survey tied in many different marine surveys as well as constraining some important data gaps. Due to the low flight altitude (∼160 m) the airborne free air anomalies have been treated directly as marine data, as downward continuation effects should be minimal (Forsberg et al. 2004).

The free-air gravity data set obtained by merging data from different institutions resulted in 1,293,236 gravity points and is shown in Fig. 1. Red lines represent airborne gravity data thinned to an along track distance of 10 km. Individual cruises originate from many different projects over a long period of time and their quality varies. Most of the data sources, these from BGI, BGS, and particularly NGDC, have detailed descriptions of all gravity surveys. The NGDC data come in MGD77 Marine Geophysical Data Exchange format, organized with one file per "survey-leg". This is directly useful for the cross-over adjustment. For other sources this information may be missing.

3 Archives, 'surveys' and the choice of adjustment model

Our adjustment involves a model with at least one parameter for every *survey*, corresponding to an optimal shift in its gravity datum. For long, well-crossed surveys, the model may add a second parameter, representing linear instrumental drift. However, we are not usually able to retrieve all the information needed to identify the real operational unit of data collection, so what we are forced to call a 'survey' has to be pragmatic and may include a range of different types of data set.

A marine survey is operationally hierarchical: a *cruise* involves a particular ship, gravity meter and survey institution. It starts at a home port, may call in at a sequence of other ports and then return to its home port at the end of a season. The data component collected between successive port visits—places where the gravity datum and instrumental drift rate may have been adjusted—is known as one *leg* of the cruise. Each leg may consist of many *lines*.

Ideally, the unit of data for which the adjustment model uses the same parameters corresponds to a leg. Throughout a leg, the gravity datum and reference system, together with the behaviour of the gravity meter, should be consistent. Ideally, what we call a *survey* should be the same as a leg. However, even good archiving structures may not record port visits, so our analysis may not be able to identify legs and, in practice, the whole cruise may be the only data component that can be distinguished objectively. In this case, the need for a different adjustment model for different parts of the same survey may become apparent after the first adjustment and some iteration that subdivides surveys and carries out a new adjustment may be necessary.

A more serious difficulty is posed by the few data archives that only list gravity and position in geographically sorted bins. In some cases these data have to be discarded but, where alternative coverage is missing, very considerable computational effort is needed using azimuth and distance criteria to reconstruct individual survey tracks, often requiring manual interaction. Even if a probable *ship track* can be identified and isolated, the direction of travel remains unknown. More seriously, not knowing how to construct a survey as a time-ordered sequence of lines means that every empirically identified line-segment has to be treated as a one-line survey. This can greatly increase the number of free parameters in the adjustment model, as well as decreasing its stability. In practice, our use of the term *survey* in relation to marine gravity data in the Northern Atlantic ranges from more than 25,000 km of ship track to a group of ten data points that we deduce were collected by the single passage of one ship.

4 Line segments, curve-fitting and a priori errors

Although the *survey* attempts to represent an operational unit of data collection and forms the basis of the network adjustment model, the basic component of our pre-processing algorithm is the *line-segment*. A line segment is a component of a survey where the ship's course is adequately straight. Successive point-to-point vectors are compared, using adopted criteria for breaking surveys into line-segments: a break can be triggered by a large change in course azimuth or an excessive gap between points. We assign to the majority of the survey a new line-segment only if the point-to-point azimuth changes by more than 6 degree and if point spacing exceeds 5km or

more. However, the point-spacing and azimuth change have to be increased in few ship-tracks.

By using only line-segment data, we improve the reliability of the data used for the network adjustment stage. During a course change, and for a period after it, the stabilised platform housing the sensor may introduce transient gravity errors. They should not modify either the instrument's long-term datum or its drift rate, so it remains appropriate to use the same drift model for the many line segments that make up a survey. However, data collected during and soon after course changes may be unreliable: we discard them.

In order to maintain an adequately uniform and isotropic representation of distance and direction—features needed here for identifying linear segments but also later for data interpolation and geoid computation—we first convert latitude and longitude into the eastings and northings of an appropriate map projection. For our region of the North Atlantic, we use a conformal Lambert conic projection with standard parallels at 55°N and 75°N. After the initial extraction of information from data archives, all other processing is carried out in map projection coordinates.

Apart from an unknown datum shift and possibly an unknown linear slope, we suppose that the gravity anomaly profile along one line segment involves 'noise' superimposed on a smooth function of along-track distance. The shape of this function should correspond to 'true' gravity. In practice, this noise results from a variety of sources—the more significant ones include failure of the stabilisation system to deal with bad sea-states and, for early surveys, digitisation binning and failure to re-process dynamical corrections once post-facto navigation corrections became known. We suppose that these components of noise can be modelled as spatially random. In addition to random noise, recording blunders and instrumental malfunction may generate spikes or unrealistic excursions.

For each line-segment, the pre-processing routine involves three operations. First, it must parametrise the smooth curve representing 'true' gravity; second, it must quantify the random noise, and, third, it must identify and remove 'blunders'. For the deep-water parts of the Northern Atlantic, we have some 12,000 line-segments, so these processes have to be largely automatic.

The first stage represents the free air anomaly, the easting and the northing as a parametric function of along-track distance using the Chebyshev polynomial curve fitting program (we have to use along-track distance as a proxy for time: time itself is rarely included in archives, although the *direction* of time is nearly always available via the contributor's point number). For the measurement positions, we use a quadratic function, rather than a linear one, in order to allow for long tracks smoothly following a line of latitude.

For the free air anomaly, the routine fits progressively higher degree Chebyshev polynomials, continuing automatically until both the standard deviation of the residuals and their largest absolute value fall below chosen limits, typically 0.5 and 1 mGal, respectively. Here the 'trick' is to devise rules that do not overfit noisy data but still give a faithful representation of 'true' gravity over the shelf-edge, canyons, sea mounts, the mid-ocean-ridge and other real features with high amplitudes and relatively short wavelengths. For any segment where the fitting criteria are not met, the software displays a profile showing the observed points, the polynomial curve and a curve interpolated from KMS02 altimetric gravity anomalies (Andersen et al. 2003). At this stage, data spikes and blunders are identified and eliminated, if necessary by manual editing. If the display brings up many instances of over- or under-fitting for the line-segments of one particular survey, the general fitting parameters may be changed but, usually, only a simple data edit is needed. Overall, only about 2% of line segments need manual intervention. Once the whole of a survey has passed these tests, the points and the fitted curves for all line segments are displayed in succession for a final visual check. Figure 2 shows an example of the verification display.

The output of the pre-processing stage is a file describing the whole of one or more surveys, but grouped into data batches for each line-segment. The main information includes the set of Chebyshev polynomial coefficients describing the free air anomaly, and the course easting and northing. For each line segment, the *RMS* misfit is recorded, playing an important role as an a priori error in the network adjustment.

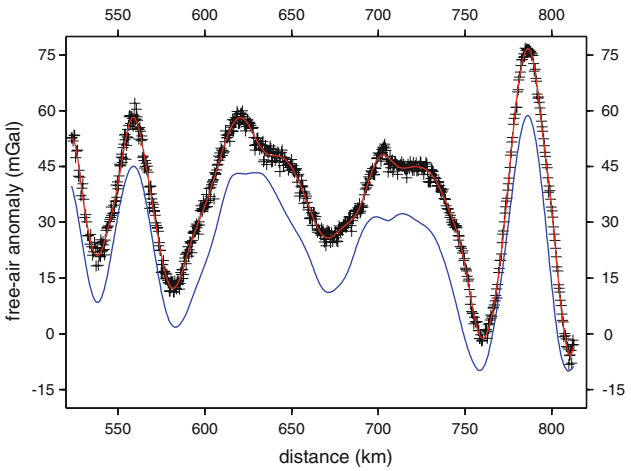

Fig. 2 Line-segment verification display. This example of a ship-track segment has high noise levels (the curve misfit has a standard deviation of 1.38 mGal and a maximum of 6.03 mGal). Although failing typical criteria of 0.5 and 1.5 mGal, the continuous curve (in *red*) was judged to be an appropriate representation of the observation points, represented by + sign. The altimetric gravity anomaly curve is shown in *blue* and illustrates a datum shift of about 10 mGal. Typically altimetric gravity anomalies have a lower resolution

In identifying and then processing all the line segments of a particular survey, the along-track distance is cumulative, including the discarded parts of the survey during course changes. Chebyshev polynomials require that their argument—along-track distance—be scaled to lie between -1 and $+1$, so the along-track distance of the first and last point on each line segment must also be recorded. There is a corresponding record of the minimum and maximum easting and northing. These values are also useful to determine quickly that two line segments do not intersect. All future processing uses just the Chebyshev polynomial coefficients, rather than the original point data.

5 Line crossing points and connectivity

A typical geodetic network is *designed*. Network design aims to achieve a particular level of accuracy, reliability and cost. It chooses what size of polygon needs to be observed, where bracing links are needed and what absolute constraints should be imposed and where. These methods are occasionally used for inshore gravity surveys prospecting locally for petroleum. There, ship tracks are usually regularly parallel and cross-lines are added for control. Commercial software for analysing cross-over errors exists for tracks with nearly orthogonal geometry and where manual selection ensures that all tracks are interconnected.

In contrast, an ocean-wide marine gravity 'network' is not 'designed', but comes about as a chance assembly of unrelated ship tracks. The network is rarely strongly braced, so single 'passage-lines' become structurally important but may involve unfavourably acute angles for track intersections. The first task is to find all the points where two line-segments cross and, at each of these points, to find the free air anomaly estimated by the two lines-segments. The next task is to identify and select only those crossing points that lie on a network that is *interconnected*.

The use of Chebyshev polynomials and the structure of the line-index file were chosen to speed up the process of identifying line-crossing points. Each line-segment is compared with every other line-segment stored below it in the file. The first test rejects intersection if the rectangles defined by the minimum and maximum easting and northing do not overlap. If they do, the next test solves for the intersection points of the *first* degree Chebyshev polynomials for easting and northing. Line-crossing is rejected if either *normalised* distance lies outside a normalised distance range of ± 1.5. If the two segments pass this test, a final exact intersection point is found iteratively using the second degree polynomials with a tangent intersection method. This is quicker and less cumbersome than a rigorous solution of the quartic equations.

Once the crossing point has been determined, we use the Chebyshev polynomials that describe the free air anomaly as a continuous function of along-track distance to estimate gravity at the intersection point. Some cross-over analysis routines use piecewise-linear interpolation to calculate this from the points along the ship track where it is measured. However, this process can alias random errors and has been shown to generate systematic geoid effects up to 50 cm over 500 km (Hipkin et al. 2004). Our routine avoids aliasing.

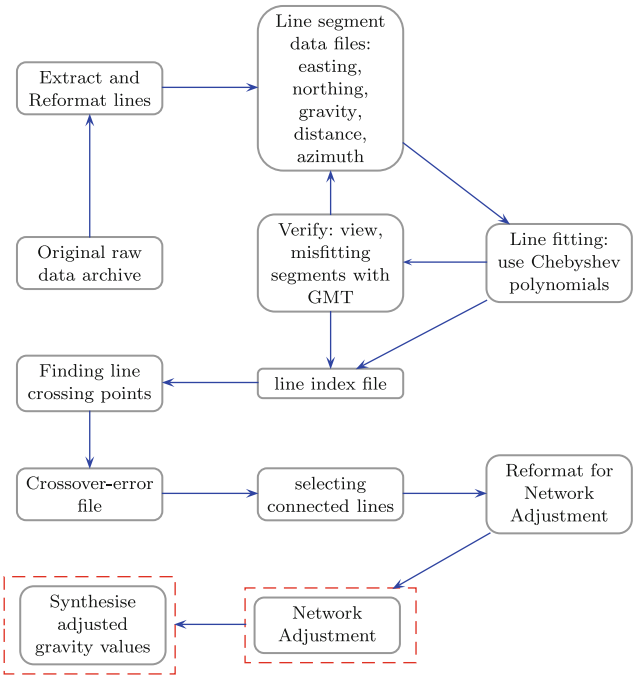

Fig. 3 The flow chart of data cleaning and adjustment procedure

The output of the line-crossing algorithm gives the survey identifier, the along-track distance, free air anomaly estimate and *rms* line-segment misfit at every crossing point. For a 3500 km square of the North Atlantic, all 41,560 crossing points in deep water were found in a few seconds. The next task is to find which surveys form part of an interconnected network. With more than 12000 line-segments, this could not be done manually. Our 'brute force' algorithm fully automates the process but it remains computationally intensive. Note that two surveys are connected if any line-segment of one crosses any line-segment of another: it is not necessary for every line-segment to contain a crossing point. This is because the adjustment involves the same model parameters for the whole of one survey. The complete data pre-processing overflow diagram is shown in Fig. 3.

6 Least-squares adjustment model

If the pre-processing stages have been successful, the gravity values obtained at cross-over points need only a *survey-dependent* modification to correct for different gravity reference systems, bad connections to harbour base stations and

instrumental drift. Determining these is the purpose of network adjustment, where estimates for each survey are modified by a one or two parameter model:

$$g_{km} - G_m - a_k - b_k s_{km} = v'_{km} \tag{1}$$

where g_{km} is the free air anomaly provided by Chebyshev polynomial fitting at intersection point m on survey k; v'_{km} is the residual for the observation on survey k at cross-over point m; G_m is the 'true' free anomaly at cross-over point m; a_k is the datum shift for survey k; b_k is the drift rate (mGal km^{-1}) for survey k, and s_{km} is the cumulative along-track distance from the beginning of survey k to cross-over point m.

It is self-evident that the set of Eq. (1) cannot be solved for the unknown parameters G_m, a_k, b_k: if one arbitrary constant is added to all the site gravity values G_m and the same one subtracted from all the survey gravity datum shifts a_k, the 'observations' g_{km} remain unchanged. Prescribing the free air anomaly for one of the cross-over sites, or fixing the datum shift for one of the surveys are alternative ways of converting this indeterminacy to *a free adjustment solution*. Fixing two or more site values could be used to generate a *constrained adjustment solution*: for example, we could impose free air anomaly values at cross-over points near Greenland and near Norway to penalise the accumulation of east-west trending errors. We have chosen a free adjustment and define the datum on one long tie line to be zero. In what follows, it is assumed that the equation set (1) has been modified to incorporate the imposition of $a_1 = 0$. We note ways of testing this proposition later. For any cross-over site m, there will be an equation like (1) for each of the two surveys whose line-segments intersect there. Commonly, cross-over adjustment algorithms subtract the two and so eliminate the cross-over point value G_m. However, the residuals on different surveys do not necessary belong to the same population of errors, so their difference will form a disparate population for which 'minimising the sum of the squares of the residuals' may not have much meaning. Our approach uses the earlier curve fitting stage to provide an a priori estimate of the standard deviation σ_{km} of each error population. We thereby convert all residuals to common population of normalised residuals v_{km}:

$$\frac{g_{km}}{\sigma_{km}} - \frac{G_m}{\sigma_{km}} - \frac{a_k}{\sigma_{km}} - \frac{b_k s_{km}}{\sigma_{km}} = \frac{v'_{km}}{\sigma_{km}} = vkm \tag{2}$$

Note that this approach allows the characteristics of the error population to vary during one survey: the standard deviation is estimated separately for each of its line-segments. If blunder and spike detection has been successful, residuals from the n observational equations will have zero mean, $\sum v_i = 0$. If the adjustment model is appropriate, residuals will be uncorrelated, that is $\sum v_i v_j = 0$ for $i \neq j$. The root mean square residual will estimate the standard error of the adjustment, $(\frac{1}{N}) \sum v_i^2 = \sigma_0^2$ and, if the normalisation has been successful in scale as well as functional form, we expect $\sigma_0^2 \approx 1$. This procedure corresponds to assuming that what geodetic literature calls the weight matrix is diagonal. More elaborate treatments are noted below but are not self-evidently appropriate for our problem; nor are they computationally viable. The matrix representation of the N observation equations, each of which depends (very sparsely!) on p unknown parameters, is, for Eq. (1)

$$\mathbf{C}' - \mathbf{D}'\mathbf{X} = \mathbf{v}' \tag{3}$$

and for Eq. (2)

$$\mathbf{C} - \mathbf{D}\mathbf{X} = \mathbf{v} \tag{4}$$

where $\mathbf{C}$ is an n-length column vector of the 'observations'; $\mathbf{D}$ is an n by p observational matrix (or 'design' matrix) whose coefficients are known; $\mathbf{X}$ is a p-length column vector of the unknown parameters, and $\mathbf{v}$ is an n-length column vector of the normalised residuals. The normal equations are derived by minimising $v^T v$ have the form

$$\mathbf{D}^T\mathbf{D}\mathbf{X} = \mathbf{D}^T\mathbf{C} \tag{5}$$

for which a simpler notation is

$$\mathbf{A}\mathbf{X} = \mathbf{B} \tag{6}$$

In principle, their solution is found from Eq. (6) as

$$\mathbf{X} = \mathbf{A}^{-1}\mathbf{B} \tag{7}$$

In practice, the size of the normal equation matrix $\mathbf{A}$ is too large for its inverse to be computed. For our work with North Atlantic data, there are about 49,000 unknown parameters, so simply writing one double precision matrix with the size of $\mathbf{A}$ would occupy about 20 Gbyte, beyond the capacity of the processor RAM. Computation of the full inverse matrix $\mathbf{A}^{-1}$ would be entirely prohibitive at the present and even a direct solution of the normal equations by, for example, Cholesky LU decomposition (Golub and van Loan 1996) remains impractical.

7 Solving the normal equations

Our algorithm avoids computing the design matrix $\mathbf{D}$ altogether and computes individual non-zero elements of the normal equation $\mathbf{A}$ directly from the output of the line-crossing program, storing the result using the Stanford row-indexed sparse-matrix algorithm (Press et al. 1986). This process needs 'smart' book-keeping. Suppose that there were originally M' cross-over points on K' surveys. When only those forming a connected network are identified, these numbers will be reduced to M sites on K surveys. There will then be at least $M + K - 1$ unknown parameters. This could potentially rise to $M + 2K - 1$ if each survey is allowed an

adjustment model with both a datum shift and an instrumental drift parameter. For small surveys with few cross-over points, the two-parameter model generates instability. We assign an instrumental drift parameter only if the along-track distance between the first and last cross-over point exceeds a chosen value, typically 2,000 km, and if number of other surveys that are intersected exceeds another chosen value, typically 10. Wessel and Watts (1988) suggested the drift rates should only be computed for 'leg-survey' with more than 100 cross-overs. Coincidently, our chosen criterion for assigning a drift parameter to a particular 'legs-survey' in our network adjustment has shown that the numbers of crossings are more than 100. Thus the number of unknown parameters finally appearing in the normal equations is determined dynamically as the processing progresses. At each stage, the parameters have to be re-indexed. Writing the normal equation matrix directly with the correct indexing for the sparse matrix storage scheme requires some subtleties. When the solution is finally available, the cascade of re-indexing has to be reversed in order to associate the right datum shift with the right survey.

The normal equations are solved using the bi-conjugate gradient with pre-conditioning (PBCG) algorithm (Press et al. 1986). The main idea of the method is that an estimate for the vector of unknown parameters is iteratively updated by adding the increment to the previous iterate. The direction of the increment is determined as the optimal direction towards the minimum error, which is the direction of the gradient of the sum of the squared misfits. For smaller pilot cases, this method produced the same solution within machine precision as the direct least squares method, but does not go through the matrix inversion. The rate of convergence, which is the crucial concern, can be improved by conditioning the linear system of equations in a preliminary step (Press et al. 1986).

8 Internal error estimation

If our pre-processing has been successful and our adjustment model corresponds to reality, residuals should have zero mean and be uncorrelated. While the model may itself be functionally correct, the procedure for estimating its parameters may still be imperfect. If, for example, the datum shift and slope of the drift curve of one survey are estimated wrongly, residuals at successive cross-over points along that survey will no longer be uncorrelated. In addition, this failure will bias the estimate of the datum and drift parameters deduced for surveys that it crosses. One approach aims to improve the parameter estimation process by changing the way the data are weighted. Here we discuss why we did not attempt to implement a formal variance–covariance matrix approach, even though the algorithms have become relatively standard.

With our procedure, known, a priori weights are introduced by pre-multiplying the observational matrix $\mathbf{D}'$ by an N by N matrix $\mathbf{p}$ that is diagonal and has elements $\mathbf{p_{ii}} = \frac{1}{\sigma_{km}}$. The normal equation matrix becomes

$$\mathbf{A} = \mathbf{D'^T p p^T D'} \tag{8}$$

An extension of this procedure that is claimed to improve parameter estimation is to include *off-diagonal* elements—*in extremis* to make the weight matrix full. In principle, the off-diagonal weight elements are *unknowns* to be determined from the data but, in practice, are usually imposed via a variance-covariance model. However it is determined, reciprocity requires that the weight matrix remains symmetrical (note that a more common convention calls $\mathbf{P} = pp^T$ the weight matrix).

Using Eq. (8) and comparing with Eqs. (1) and (2) makes clearer how the physical basis of the model is changed by a non-diagonal weight matrix. This we explore here. Suppose that there are M sites and K surveys; for simplicity suppose also that all surveys have a drift parameter. The i^{th} observational equation (1) can be written as

$$\sum_{m=1}^{M} \alpha_{im} G_m + \sum_{k=1}^{K} \beta_{ik}[a_k + b_k s_{km}] = g_i - v_i \tag{9}$$

With this form, where $\{\alpha_{im},\ \beta_{ik}\}$ are *unknown* parameters, the ith gravity observation now depends, *in principle*, on the value of gravity at all sites and on the datum and drift parameters of every survey. The restricted form we have used merely assigns zero to the factors α_{im} and β_{ik}, unless the ith observation is at site m and on survey k, when they are unity. What happens if this restriction is removed and all the unknowns $\{\alpha_{im}G_m,\ \beta_{ik}a_k,\ \beta_{ik}b_k\}$ become free, independent parameters? The equations become thoroughly under-determined because now there would be $M + 2K$ independent unknown parameters for *every one* of the N observations.

However, this is essentially the dilemma faced by introducing a weight matrix that is full. Suppose we continue to restrict α_{im} and β_{ik} to be zero unless the ith observation is on survey k at site m. If there are a total of N observations, pre-multiplication of the design matrix and the vector of observations by the unknown weight matrix $\mathbf{p}$ change the ith observational equation to

$$\sum_{j=1}^{N} p_{ij} \left[\sum_{m=1}^{M} \alpha_{jm} G_m + \sum_{k=1}^{K} \beta_{jk} \left(a_k + b_k s_{km}\right) \right] = \sum_{j=1}^{N} p_{ij} \left(g_j - v_j\right) \tag{10}$$

This equation has the same difficulties as the unrestricted form of Eq. (8): n linear combinations are related to $N \times (M + 2K)$ unknowns.

In other problems, a solution is found by modelling the behaviour of the p_{ij}. The weight matrix element p_{ij} essentially describes how the error distribution at point i depends on that of point j. A model may involve p_{ij} tending to zero as the distance or time interval between points i and j increases. With some data structures, this would make the weight matrix band-diagonal and the number of free parameters be much smaller. Even if some physically sensible way of modelling the error covariances did suggest itself for our problem—and so far it has not—most formal procedures then need to evaluate the inverse of the normal matrix **A**: for us this remains computationally prohibitive at the present.

We are thus unable to determine formal *internal* errors on the output of our network adjustment at the present. Fortunately, there are a number of external comparisons against which it can be tested. In addition, there are some internal tests of the validity of the model and the hypotheses used to implement it. However, we are studying a new Monte Carlo integration method to overcome the huge computational burden. In particular Gibbs sampler will be adopted to compute the inverse of the normal equation matrix.

9 Cross-over residuals

Measures of self-consistency depend on the mismatch at points where different ship tracks cross. Without some kind of processing to interpolate between points where the ship recorded gravity, the cross-over error cannot be estimated; thus, this statistic is not available for raw data. With our algorithm, we only find out where these points are after all processes of breaking up ship tracks into line-segments, discarding sections related to course changes, and then fitting continuous functions to estimate the measurement position and 'true' gravity. The most primitive cross-over statistic comes directly from the two estimates of free air anomaly at site m, g_{m1} and g_{m2}, each of which comes with an estimate of its standard deviation, σ_{m1} and σ_{m2}. With no weighting, the only estimate for site gravity is

$$G_m = \frac{1}{2}\left(g_{m1} + g_{m2}\right) \tag{11}$$

The root mean square residual for M cross-over points is

$$\sigma_r = \sqrt{\frac{\sum_{m=1}^{M} \frac{1}{2}\left(g_{m1} - g_{m2}\right)^2}{M}} \tag{12}$$

With weighting, site gravity is estimated as

$$G_m = \frac{\sigma_{m2}^2 g_1 + \sigma_{m1}^2 g_2}{\sigma_{m1}^2 + \sigma_{m2}^2} \tag{13}$$

The root mean square weighted residual is

$$\sigma_{rw} = \sqrt{\frac{\sum_{m=1}^{M} \frac{\left(g_1 - g_2\right)^2}{\sigma_{m1}^2 + \sigma_{m2}^2}}{\sum_{m=1}^{M} \frac{1}{\sigma_{m1}^2} + \frac{1}{\sigma_{m2}^2}}} \tag{14}$$

Table 1 shows the large improvement due to cleaning the input data compared with its raw state and then a further big improvement due to the network adjustment. Figure 4 shows the residual distributions before and after adjustment. Achieving data with zero mean is a necessary feature of least-squares analysis, so here the value of −0.009 mGal is not indicative of quality. However, the improvement in the unweighted standard deviation from 4 to 1.6 mGal measures the scatter remaining in the data synthesised from the Chebyshev polynomials. Since applications use *unweighted* gravity anomalies, this is a measure of local noise introduced into for example geoid computation. On a *regional* scale, network adjustment seeks to control the way errors accumulate, which translates into long wavelength geoid errors. Error accumulation depends on the *weighted* standard deviation, now reduced by the adjustment from 1.32 to 0.39 mGal.

10 External comparisons

Here we present two comparisons with external data not included in the adjustment. The first is the KMS02 synthetic free air gravity anomaly model (Andersen et al. 2003) derived from satellite altimetry. We have interpolated this on to along-track measurement points at 2 km intervals. A synthetic altimetric anomaly will have regional biases due to the effect of mean dynamic sea surface topography. Using dynamic ocean

Table 1 Descriptive statistics of the raw data and cross-over point values before and after the network adjustment (units in mGal)

Parameter	All data set	Cross-over points	
	Before pre-processing	Before adjustment	After adjustment
Number of points	1293236	83120	83120
Mean	−7.66	0.86	−0.009
SD	–	4.03	1.58
Weighted SD	61.98	1.32	0.39
Min	−84.77	−69.87	−37.73
Max	205.82	68.64	38.24

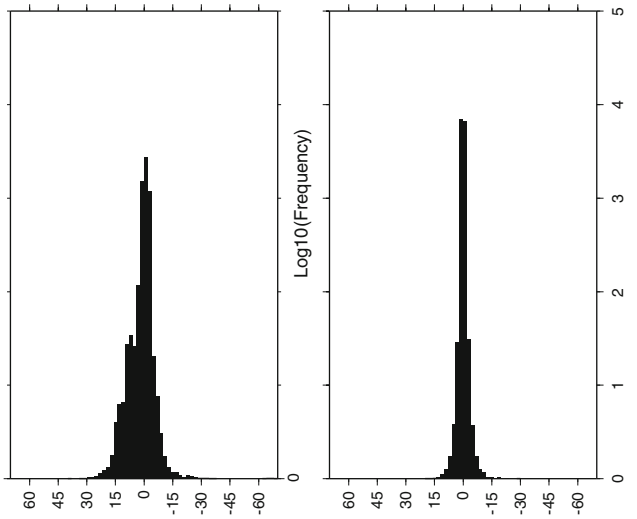

Fig. 4 Histogram of cross-over errors before (*left*) and after adjustment (*right*)

topography models derived from hydrographic data shows that the equivalent gravity signal has a range of about 2 mGal and that the biases should average to zero on a basin-wide scale. Thus comparison of well adjusted real gravity data with a good altimetric gravity model should have a mean close to zero and a standard deviation no more than 2 mGal worse than the errors in the real data. The left-hand side of Table (2) shows that the mean difference has indeed been reduced to nearly zero and the standard deviation has been reduced from 7.17 to 4.53 mGal. Similar results from comparison of shipborne and altimetric gravity data were obtained by other researchers, e.g., RMS differences of 8.5 mGal (Featherstone 2003), 5.8 mGal (Andersen and Knudsen 1998), 3–7 mGal (Sandwell and Smith 1997), and 6.12 mGal (Soltanpur et al. 2007). The extrema are larger than anticipated but mainly due to localised very high amplitude anomalies like sea mounts where neither data set will necessarily represent the correct position or amplitude of the peak.

A second comparison uses the GRACE global gravity model ggm01s (www.csr.utexas.edu/grace). This does not resolve features with wavelength less than ∼350 km and still has significant errors at ∼500 km. However, it does contain the best currently available gravity information at still longer wavelengths. In interpolating GRACE on to the measured along-track points, there will be a gross mismatch in scale—4 km (full wavelength of our marine gravity resolution) compared with 500 km. Thus most of the residuals will represent omission errors in GRACE. Because the along-track data is not available on a complete grid, it cannot be smoothed reliably to make it represent only equivalent long wavelengths. However, the surface data are available in a region about 3000 km square, large enough for the mean contribution of shorter wavelength features to vanish. We therefore expect that comparison with GRACE will identify any datum error in the adjustment values, but that little information will be contained in the standard deviations, or extrema. The right-hand side of Table 2 confirms these expectations. Note that we have carried out a free adjustment, in which the datum correction of only one ship-track fixes the level of the whole of the northern Atlantic. This survey was chosen carefully: although it is an unidentified military passage line, it runs between harbour ties in Svarlbard, the Faroes and Iceland, thereby controlling most of the central part of the Nordic Seas and the long wavelength datum. This datum differs from the global datum of GRACE by only 0.0068 mGal.

11 Mean Dynamic Topography in the northern North Atlantic

The advance that allows us to create purely geodetic images of ocean currents comes from being able to compute a very much better marine geoid. Although the GRACE mission played some part, the big improvement comes from a systematic and ocean-wide adjustment of marine gravity at some 1.3 million points along ship-tracks, combined with a novel way of using satellite altimetry to fill between-track gaps.

Geostrophic currents in the uppermost part of the ocean can be determined by the slope of the ocean's Dynamic Topography (DT). The DT, ζ, is observed as the difference of altimetric sea surface height, h and the geoid, N. After averaging over time, mean values are then related by

$$\overline{h} = N + \overline{\zeta} \tag{15}$$

Mean Dynamic Topography (MDT), $\overline{\zeta}$ can differ from the geoid with slopes up to a few decimetres over distances of 100 km. While the time-averaged Mean Sea Surface Height

Table 2 Descriptive statistics of the difference between surface gravity and external data, both evaluated at 2 km intervals along observation tracks (mGal)

Parameter	Altimetric free air anomalies		GRACE free air anomalies	
	Before adjustment	After adjustment	Before adjustment	After adjustment
Mean	2.27	0.009	2.31	0.007
SD	7.17	4.53	17.68	16.82
Min	−84.29	−64.68	−107.76	−102.94
Max	70.44	59.47	205.82	203.76

(MSSH) $\overline{h}$ is known to a few centimetres (e.g., Wunsch and Stammer 1998; Chelton et al. 2001; Tapley and Kim 2001; Andersen et al. 2003; Rio and Hernandez 2004), existing global geoid models, based on a combination of surface and space-borne gravimetry, have provided only decimetric accuracy (Johannessen et al. 2003). Consequently, calculating MDT by differencing MSSH and the geoid has not hitherto been successful at shorter wavelengths (Wunsch and Stammer 1998). Improvements in the accuracy (∼1 cm) and resolution (∼100 km) of space geodetic MDT are expected after the launch of the GOCE satellite. Here we have used the MSSH models KMS04 (cf KMS02 Andersen et al. 2003) and CLS04 (cf CLS01 Rio and Hernandez 2004). The models are global on a 2 min grid. The two models agree over the North Atlantic Ocean with a standard deviation of 2.7 cm.

However, some regions, like the northern North Atlantic, already have a sufficiently dense coverage of gravity data to estimate a regional geoid with the accuracy needed to estimate MDT and at better resolution than even forthcoming gravity satellite missions. (Because the gravity power spectrum increases rapidly with wavelength, a complete geoid cannot be found with surface data alone—the longest wavelengths need further constraint: we generated free air gravity anomalies Δg by filtering surface data to suppress the very long wavelengths better represented by GRACE's global model (Tapley et al. 2004). Proper use of the resource provided by marine gravity data has two benefits: first, the 'geodetic' MDT contains valuable higher resolution information about the ocean's dynamical system and, second, the geoid could serve as reference for calibration or validation of GOCE gravimetric data. The next section describes how ship and airborne data can be incorporated into regional geoid computation.

11.1 Iterative combination method

Our MDT model derived from geodetic data comes from modifying an initial a priori oceanographic MDT model in two steps: first, we make its long wavelength structure consistent with satellite altimetry combined with the reliable parts of the geoid as deduced from GRACE observations; second, we add shorter wavelength information coming from surface gravity data. However, the second task is neither linear nor independent. The problem is not just an evaluation of Eq. (15) to get an optimal estimate of the two independent quantities directly from observations of all three because the geoid is not an observable. Computing a gravimetric geoid, N involves a surface integral of gravity, meaning that gravity coverage must be complete. The cleaned and adjusted surface observations provide a strong gravity field constraint but only along survey lines. Our Iterative Combination Method (ICM) (see also Hipkin and Hunegnaw 2006) is a conceptually rigorous way of filling in the gaps between them to create a complete gravity grid.

Network adjustment demonstrated that surface gravity anomalies data are inherently accurate. However, a purely empirical interpolation into the data gaps between survey tracks generated gross geoid errors with unrealistic bumps many decimetres in size. An alternative approach, filling in the gaps with synthetic gravity generated from sea surface altimetry, effectively approximates Eq. (15) by ignoring MDT or replacing it by an a priori long-wavelength model.

The ICM approach combines three data streams: (1) gravity anomalies, Δg , determined with high accuracy by our cleaning and adjustment algorithms but only available along survey lines; (2) satellite altimetry giving an effectively complete coverage of MSSH, $\overline{h}$; and (3) an initial MDT model, $\overline{\zeta}$, comes from a global ocean circulation model, such as CLS (Collecte, Localisation, Satellites) combined MDT, *Rio03* (Rio and Hernandez 2004).

By treating MSSH, $\overline{h}$, as if it were derived from a potential in the same way that the geoid height, N, is derived from the anomalous gravity potential, the differential transformation from potential to gravity generates a pseudo-gravity anomaly. Using Eq. (15) we can replace

$$\Delta \mathrm{g} \approx \mathrm{g}\frac{\partial N}{\partial z} \tag{16}$$

by

$$\Delta \mathrm{g}_{\mathrm{obs}} \approx \mathrm{g}\frac{\partial \overline{h}}{\partial z} - \mathrm{g}\frac{\partial \overline{\zeta}}{\partial z} \tag{17}$$

The first term on the right-hand side of Eq. (17) is the pseudo-gravity anomaly, $\Delta \mathrm{g}_{PS}$. It is systematically different from the real gravity anomaly Δg. Computing the difference from oceanographic estimates of MDT shows that it reaches ∼2 mGal (1 mGal = 10^{-5} m s^{-2}) and appears to be dominated by wavelengths more than 100 km. However, both its apparent smoothness and its limited amplitude may be a spurious consequence of the low resolution of oceanographic models. The spectral characteristics of real MDT are not well known.

Physical geodesy normally uses the inverse of Eq. (16), which implicitly uses Laplace's equation to replace a derivative or integral over the vertical coordinate z by horizontal derivatives or an area integral over the horizontal surface

$$N = \int\int F \Delta \mathrm{g}\, \mathrm{d}s \tag{18}$$

F is the Stokes kernel function relating a gravity anomaly at one point to its geoid contribution at another. In Eq. (18) we can substitute either a real gravity anomaly for Δg, or a synthetic version derived from the two terms on the right-hand side of Eq. 17, or a weighted combination of the two. The weighted combination allows us to create a complete

grid of gravity anomalies so that Eq. (18) gives a complete grid of geoid heights.

The process, which has to be iterative because $\overline{\zeta}$ is initially unknown and is the quantity being sought, is described by

$$\overline{h} - \overline{\zeta}_{i+1} = \int\int F \left[\frac{w_G \Delta g + w_A g \left(\frac{\partial \overline{h}}{\partial z} - \frac{\partial \overline{\zeta}_i}{\partial z} \right)}{w_G + w_A} \right] ds \quad (19)$$

We start by using an initial estimate for $\overline{\zeta}$, derived from a global circulation model, for the right-hand side of Eq. (19) to get a revised estimate of MDT on the left hand side. Here, the altimetric sea surface $\overline{h}$ is considered known. Integration and differentiation use a Fast Fourier Transform technique. Equation (19) represents this iterative loop that continues until the interpolation of gridded gravity back on to the survey tracks adequately reproduces the measured along-track gravity. The routine uses two grids of weights. The altimetry weight, w_A, is set to zero on land and unity over the oceans with a smooth transition across the coast. The surface gravity weight, w_G, is unity on land but, offshore, is assigned a value that decreases rapidly away from survey tracks. w_G is computed at each grid point as the sum of a contribution from every marine or airborne gravity observation. Each contribution decreases with distance from the observation point in a way that matches the gravity effect of a point mass. These contributions are also scaled by the standard deviation of the survey data along each survey line (see Sect. 6)

The ICM algorithm has two equivalent outputs: a grid of final MDT values and a grid of composite gravity anomalies. The iterative scheme converges rapidly, generally with a good solution after a couple of iterations. After ten iterations, the rms incremental change per iteration is less than 3 mm for the MDT model and less than 0.04 mGal for gravity. The result was found to be relatively insensitive to the choice of the initial oceanographic starting model: the standard deviation of differences between the ICM output using initial MDTs derived from four different global ocean circulation models ranged from 1.9 to 2.6 cm. The final ICM MDT model is shown in Fig. 5 smoothed with a Gaussian low-pass filter whose sigma was 25 km sigma.

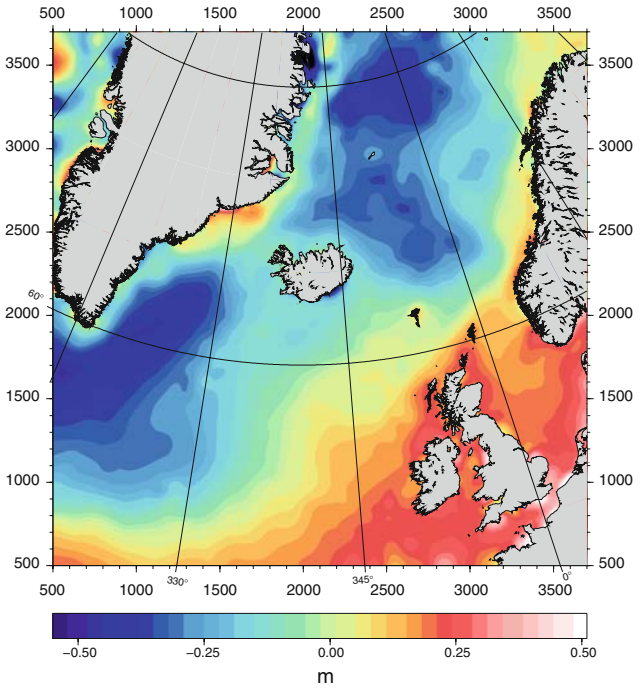

Fig. 5 MDT model smoothed with a $\sigma = 25$ km Gaussian low-pass filter

12 Geostrophic currents

To validate the surface circulation resulting from the ICM MDT (Fig. 5) we use current estimates deduced from drifting buoys deployed in the World Ocean Circulation Experiment (WOCE) Surface Velocity Program (SVP). The experiment used the ARGOS system to locate buoys periodically via-polar orbiting NOAA satellites and so gave water displacement directly (Niiler et al. 1995). The drifters consist of a surface float and a drogue connected to a tether at a depth of 15 m (Sybrandy and Niiler 1990). The slippage of the drogue drifters through the water due to transfer of momentum to the surface buoy from waves and wind is minimised through their design and estimated to be less than 0.1% of the wind speed (Niiler and Paduan 1995).

The data used in the present study were quality-controlled and optimally interpolated to create a uniform time series of positions at six-hour intervals. First, outliers were removed by a despiking program and the despiked data interpolated over 2-h intervals (Hansen and Poulain 1996). The interpolated positions were then low pass filtered with a cut off period at 36 h in order to reduce high frequency components of tidal and inertial currents (Otto and van Aken 1996). The resulting positions were then sub-sampled every 6 h (www.aoml.noaa.gov). For our analysis we only used those parts of the position time series when the drogue was attached to the drifter, some 1111 WOCE/TOGA type drifters in the northern North Atlantic during the period 1990–2006. Figure 6 shows the erratic displacements filtered in Fig. 8 to show a small steady state flow.

Figure 7 shows our geodetic version of the time-averaged geostrophic currents as predicted by the ICM MDT shown in Fig. 5. Figure 8 displays a corresponding circulation derived from filtered Lagrangian buoy trajectories estimated for a depth of 15 m. The geodetic and drifting buoy methods give remarkably similar results. They agree in the location of the strong currents along the western, southern and eastern

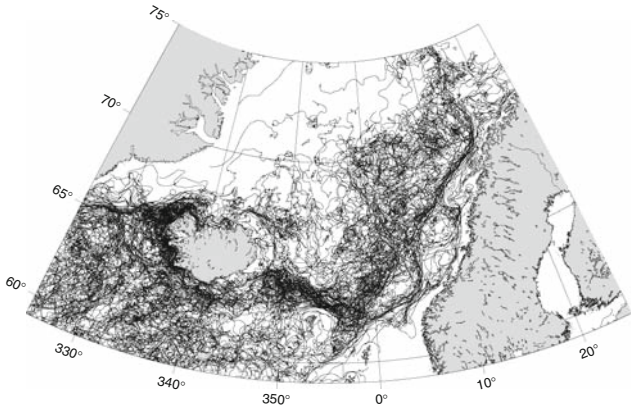

Fig. 6 Trajectories of drifters in 1990–2006, drogued at 15 m

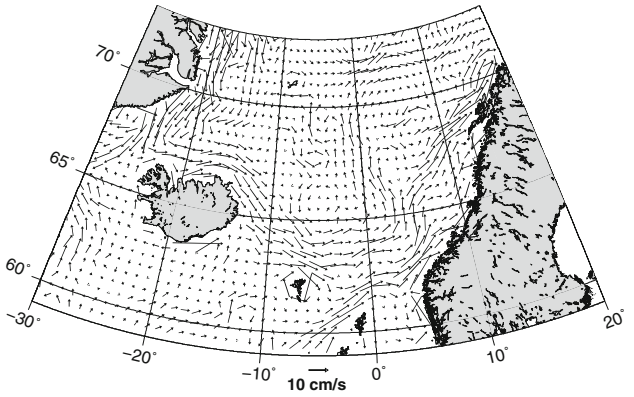

Fig. 7 The geostrophic currents as deduced from the ICM MDT

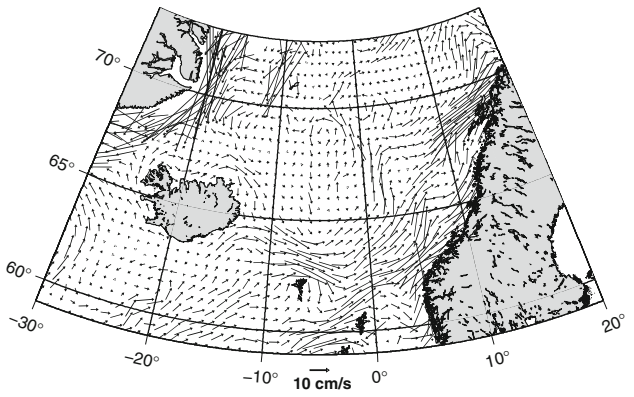

Fig. 8 The currents at 15 m depth deduced from Lagrangian drifters

margin of the Nordic Seas. All three branches of the Norwegian Atlantic Currents are reproduced in the flow deduced from the ICM MDT, including the bifurcation of the westernmost branch at 68°N ; there, most of the water flows northward towards the Fram Strait but part of it follows the southern rim of the Lofoten Basin eastward towards the coast of Norway. Even the small current southward at 7°W approximately following the 2,000 m isobath between the Iceland and the Norwegian Basins is reproduced. However the peak velocities in the ICM MDT currents are generally lower than those observed from the drifter data. This is may be attributed to the smoothing we applied to reduce noise which attenuates our peak velocities and spreads the same flow over a wider region. In particular, the ICM MDT estimate of the North Atlantic Drift north-eastwards at (18°W, 60°N) towards the Iceland-Faroe Ridge is too low compared with observations. However, the strong southward flow in the Greenland Sea at 10°W indicated from the drifters, which we do not find in our geodetic estimate, is probably a transient phenomenon. This is supported by results from Jakobsen et al. (2003) who also do not find it in their drifter results for the period 1990–2000 (Fig. 5) (not shown); otherwise their circulation map is similar to ours derived from the extended drifter data set (Fig. 8).

The ability of the ICM MDT model to predict the velocity of drifting buoys was also tested during a CLS validation experiment (Rio 2005, personal communication). The results from 172,920 observations of buoy velocities for the period 1993–2003 were compared with predicted instantaneous velocities. The latter came from an instantaneous velocity anomaly deduced from satellite altimetry, set against a background of the geostrophic velocity deduced from an MDT model. Their experiment has been repeated with three MDT models for the mean flow: ECCO (Estimating the Circulation and Climate of the Ocean) (Stammer et al. 2002) and Niiler (Niiler 2001), and the ICM MDT (Hipkin and Hunegnaw 2006). Table 3 shows the rms of the east–west and north–south components of velocity difference and a vectorial correlation coefficient (Rio 2005, personal communication). Not surprisingly, the best model is the Niiler MDT, which was itself deduced from the drifter data. However, the ICM MDT does better than the MDT derived from ECCO even though surface drifter data are assimilated in the state estimation procedure.

Table 3 Validation results for different models of the mean flow (Rio 2005, personal communication)

Parameter	RMS east velocity V_E (cm s^{-1})	RMS north velocity V_N (cm s^{-1})	Vector correlation coefficient R_c
ICM MDT	11.2	10.5	0.47
Niiler	11.1	10.4	0.50
ECCO	11.5	11.2	0.41

13 Discussion

With our systematic approach to cleaning and adjusting very large compilations of marine gravity data, and by adding the control provided by modern airborne gravity lines, we have generated a very accurate ocean-wide gravity data set whose quality has been demonstrated. This verification has had to be by external comparison because, at the present time, the size of the matrix adjustment stage makes formal internal error estimation and error propagation computationally prohibitive. The work described in this paper solves two problems associated with marine geoid computations: the supposed inaccuracy of marine gravity anomalies and gaps in their coverage. Figure 1 shows that, even in the unusually favourable circumstances of the northern North Atlantic, there are still large data gaps. Our Iterative Combination Method (ICM) algorithm has been able to generate complete grids of gravity and Mean Dynamic Topography (MDT) that are mutually consistent from this incomplete coverage of gravity. It combines surface gravity with satellite altimetry and trial oceanographic data, and uses integral properties of the gravity field derived from potential theory. This result is insensitive to the choice of initial oceanographic model.

The ICM-based estimate of geostrophic currents breaks new ground by identifying high resolution features matching those of the best regional models based on hydrography and Lagrangian drifters (Pickart 2000; Jakobsen et al. 2003). The resolution exceeds that expected from forthcoming gravity satellite missions. We report validation experiments with drifters showing that our geodetic predictions of geostrophic currents match or exceed the performance of global ocean circulation models.

Hitherto, the poor accuracy and resolution of marine gravimetric geoids has made the contribution of a geodetic MDT to oceanography at best marginal. The work we report on the northern North Atlantic changes that and the increase in accuracy represents a breakthrough: for the first time, gravimetric methods are able to provide a new level of detail and completeness of coverage to oceanographic models.

Acknowledgments This work was carried out as part of the EU contract (EVK2-CT-2002-00077) entitled 'Gravity and Ocean Circulation in the North Atlantic (GOCINA)'. The authors thank partners in the Danish and Norwegian mapping agencies, KMS and SK, and the British Geological Survey (Permission IPR/26-42C) for sharing access to gravity survey data. We also thank Generic Mapping Tools (GMT) developers (Wessel and Smith 1995).

References

Adjaout A, Sarrailh M (1997) A new gravity map, a new marine geoid around Japan and the detection of the Kurosho current. J Geod 71:725–735

Andersen OB, Knudsen P (1998) Global marine gravity field from the ERS-1 and Geosat geodetic mission altimetry. J Geophys Res 103(C4):8129–8137

Andersen OB, Knudsen P, Kenyon S, Trimmer, R (2003) KMS2002 Global marine gravity field, bathymetry and mean sea surface. Poster, International Union of Geodesy and Geophysics General Assembly, Sapporo, Japan, June 30–July 11

Bell E, Watts AB (1986) Evaluation of BGM-3 sea gravity meter system onboard R/V Conrad. Geophysics 51(7):1480–1493

Catalao J, Sevilla MJ (2004) Inner and minimum constraint adjustment of marine gravity data. Comput Geosci 30:949–957

Chelton, DB, Ries JC, Haines BJ, Fu LL, Challahan PS (2001) In: Fu LL, Cazenave A (ed) Satellite altimetry and earth sciences. Academic Press, San Diego, pp 1–131

Denker H, Ronald M (2003) Compilation and evaluation of a consistent marine gravity data set surrounding Europe. Proc IUUG, Soporo, Japan, June 30–July 11

Drinkwater MR, Floberghagen R, Haagmans D, Muzi PA (2003) GOCE: ESA's first Earth Explorer Core mission. Space Sci Rev 108:419–432

Featherstone WE (2003) Comparison of different satellite altimetric-derived gravity anomaly grids with ship-borne gravity data around Australia. In: Tziavos IN (ed) Gravity and Geoid-3rd Meeting of the international Gravity and Geoid Commission, Greece, August 26–30, 2002

Forsberg R, Olesen A, Vest A, Solheim D, Hipkin R, Omang O, Knudsen P (2004) Gravity field improvements in the North Atlantic region for the GOCINA project. 2nd International GOCE user workshop. ESA, ESRIN, March 8–10

Golub G, Loan Cvan (1996) Matrix computations, 3rd edn. Johns Hopkins University Press, London

Hansen D, Poulain PM (1996) Quality control and interpolations of WOCE-TOGA drifter data. J Atmos Oceanic Technol 13:900–909

Hipkin R, Haines K, Beggan C, Bingley R, Hernandez F, Holt J, Baker T (2004) The geoid EDIN2000 and mean sea surface topography around the British Isles. J Geophys Int 157:565–577

Hwang C, Wang C, Lee L (2002) Adjustment of relative gravity measurements using weighted and datum free constraints. Comput Geosci 28(9):1005–1015

Hipkin R, Hunegnaw A (2006) Mean dynamic topography by an iterative combination method. In: Knudsen P, et al. (eds) Proceedings of the workshop: GOCINA: IMproving modelling of ocean transport and climate prediction in the North Atlantic region using GOCE gravimetry, Cah Cent Eur Geod Seismol, 25, pp 135–140

Johannessen JA, Balmino G, Le Provost C, Rummel R, Sabadini R, Sunkel H, Tscherning CC, Visser P, Woodworth P, Hughes C, LeGrand P, Sneeuw N, Perosanz F, Aguirre-Martinez M, Rebhan H, Drinkwater M (2003) The European gravity field and steady state ocean circulation explorer satellite mission: impact in geophysics. Surv Geophys 24:339–386

Jakobsen PK, Ribergaard M, Quadasel D, Schmith T, Hughes CW (2003) Near-surface circulation in the northern North Atlantic as inferred from lagrangian drifters: Variability from the mesoscale to inter-annual. J Geophys Res 108(C8), 3251. doi:10.1029/2002JC001554

Lemoine F, Kenyon SC, Factor JK, Trimmer RG, Pavlis NK, Chinn, DS, Cox CM, Klosko SM, Luthcke SB, Torrence MH, Wang YM, Williamson RG, Pavlis EC, Rapp, RH, Olson TR (1998) The Development of the Joint NASA GSFC and the National Imagery and Mapping Agency (NIMA) Geopotential Model EGM96, NASA/TP-1998-206861

Matao H (1995) Marine gravity surveying line system adjustment. J Geod 70:158–165

Niiler PP, Sybrandy A, Bi K, Poulain P, Bitterman D (1995) Measurements of the water-following capability of holey-sock and TRISTAR drifters. Deep Sea Res 42:1951–1964

Niiler PP, Paduan JD (1995) motions in the northeast Pacific as measured by Lagrangian drifters. J Phys Oceanogr 25:2819–2830
Niiler PP (2001) In: Church J, Siedler G, Gould J (eds) The world ocean surface circulation in ocean circulation and climate-observing and modelling the global ocean, pp. 193–204. Elsevier, New York
Nishimura CE, Forsyth DW (1988) Improvements in navigation using seabeam crossing errors. Mar Geophys Res **9**:333–352
Orvik KA, Niiler P (2002) Major pathways of Atlantic water in the northern North Atlantic and Nordic Seas toward Arctic. Geophys Res Lett 29:1896
Otto L, van Aken HM (1996) Surface circulation in the northeast Atlantic Ocean as observed with drifters. Deep Sea Res I 43:467–499
Pickart RS (2000) Is Labrador Sea water formed in the Irmingar Sea?. WOCE Newsl 39:6–8
Press WP, Flannery BP, Teukolsky SA, Vetterling WT (1986) Numerical recipes in FORTRAN 90, 2nd edn. Cambridge University Press, New York
Reigber C, Schwintzer P, Neumayer KH, Barthelmes F, Konig R, Forste C, Balmino G, Biancale R, Lemoine JM, Loyer S, Bruinsma S, Perosanz F, Fayard T (2003) The CHAMP-only Earth gravity field model EIGEN-2. Adv Space Res 31:1883–1888
Rio MH, Hernandez F (2004) A mean dynamic topography computed over the world ocean from altimetry, in situ measurements, and a geoid model. J Geophys Res Oceans 109:C12032
Sandwell DT, Smith WHF (1997) Marine gravity anomaly from Geosat and ERS 1 satellite altimetry. J Geophys Res 102(B5):10039–10054
Soltanpur A, Nahavandchi H, Ghazavi K (2007) Recovery of marine gravity anomalies from ERS1, ERS2 and ENVISAT satellite altimetry data for geoid computations over Norway. Stud Geophys Geod 51:369–389
Stammer D, Wunsch C, Giering R, Eckert C, Heimbach P, Marotzke J, Adcroft A, Hill CN, Marshall J (2002) Global ocean circulation during 1992–1997, estimated from ocean observations and a general circulation model, J Geophys Res **107**(C9):3118. doi:10.1029/2001JC000888
StrangVan Hees GL (1983) Gravity Survey of the North Sea. Mar Geod 6(2):167–182
Sybrandy AL, Niiler PP (1990) The WOCE/TOGA Lagrangian drifter construction manual. Scripps Institution of Oceanography, University of California, San Diego, Ref 91/6, WOCE Report Number, 63, 58 pp
Talwani M (1971) In: Maxwell A (ed) Gravity in the sea, vol 4, part 1. John Wiley, New York, pp 251–297
Tapley BD, Kim MC (2001) Application to Geodesy. In: Fu LL, Cazenave (eds) Satellite altimetry and earth sciences, Int. Geophys. Ser., vol 69. Academic Press, New York, pp 371–403
Tapley BD, Bettadpur S, Ries JC, Thompson PF, Watkins MM (2004) GRACE measurements of mass variability in the Earth system. Science 305(5683):503–505
Torge W (1989) Gravimetry. De Gruyter, Berlin, New York
Wenzel HG (1992) Sea gravity data adjustment with program SEAGRA. Bureau Gravimetrique International, Bulletin d'Information 71:59–70
Wessel P, Watts AB (1988) On the accuracy of marine gravity measurements. J Geophys Res 93(B1):393–413
Wessel P (1989) XOVER: a cross-over error detector from track data. Comput Geosci 15(3):333–346
Wessel P, Smith WHF (1995) New version of the Generic Mapping Tools released, EOS, Transactions of the American Geophysical Union 72(441):445–446
Wunsch C, Stammer D (1998) Satellite altimetery, the marine geoid and the oceanic general circulation. Annu Rev Earth Planet Sci 26:219–254